Bonding and Redox Properties of $[Os_3(CO)_9(tmbp)(L)]$ (tmbp = 4,4′,5,5′-tetramethyl-2,2′-biphosphinine; L = CO, PPh_3) Clusters with an Unprecedented Electron-Deficient Metallic Core and Doubly Bridging Biphosphinine Dianion

Maarten J. Bakker,[a] Frank W. Vergeer,[a] František Hartl,*[a] Patrick Rosa,[b] Louis Ricard,[b] Pascal Le Floch,[b] and Maria J. Calhorda[c, d]

Abstract: Herein we describe in detail the bonding properties and electrochemical behavior of the first known triosmium carbonyl clusters with a coordinated redox-active ligand 4,4′,5,5′-tetramethyl-2,2′-biphosphinine (tmbp), the phosphorus derivative of 2,2′-bipyridine. The clusters investigated were $[Os_3(CO)_{10}(tmbp)]$ (**1**) and its derivative $[Os_3(CO)_9(PPh_3)(tmbp)]$ (**2**). The crystal structures of both clusters are compared with those of relevant compounds; they served as the basis for density functional theory (DFT and time-dependent DFT) calculations. The experimental and theoretical data reveal an unexpected and unprecedented bridging coordination mode of tmbp, with each P atom bridging two metal atoms. The tmbp ligand is formally reduced by transfer of two electrons from the triangular cluster core that consequently lacks one of the metal–metal bonds. Both **1** and **2** therefore represent $50e^-$ clusters with a coordinated $8e^-$ donor, $[tmbp]^{2-}$. The HOMO and LUMO of **1** and **2** possess a predominant contribution from different π*(tmbp) orbitals, implying that the lowest energy excited state possesses a significant intraligand character. This is in agreement with the photostability of these clusters. DFT calculations also predict the experimentally observed structure of **1** to be the most stable one in a series of several plausible structural isomers. Stepwise two-electron electrochemical reduction of **1** and **2** results in dissociation of CO and PPh_3, respectively, and formation of the $[Os_3(CO)_9(tmbp)]^{2-}$ ion. The initially produced radical anions of the parent clusters, in which the odd electron is predominantly localized on the tmbp ligand, are sufficiently stable at low temperatures and can be observed with IR spectroelectrochemistry. The electron-deficiency of the cluster core in **1** permits facile electrocatalytic substitution of a CO ligand by tertiary phosphane and phosphite donors.

Keywords: cluster compounds · density functional calculations · osmium · P ligands · spectroelectrochemistry · X-ray diffraction

Introduction

Reversible rearrangement processes in transition metal (carbonyl) clusters, selectively triggered by an external stimulus such as pH change, light absorption, or redox reaction, are important research objectives not only from the perspective of the historical role of these compounds as promising multiple-site homogeneous catalysts (in particular in fine chemistry) or as models for heterogeneous catalytic sites on metal surfaces. At least equally challenging in our opinion is their possible integration as key components (subunits) into a variety of complex supramolecular (nanometer-sized) systems where they may have specific functions, for example control of electron/energy transport across the system by reversibly changing their electronic and structural properties. For this reason, transition metal clusters with redox active ligands as chromophores and redox centers have attracted our attention since the mid 1990s, as the energeti-

[a] Dr. F. Hartl, Dr. M. J. Bakker, Dr. F. W. Vergeer
Institute of Molecular Chemistry
Universiteit van Amsterdam, Nieuwe Achtergracht 166
1018 WV Amsterdam (The Netherlands)
Fax: (+31) 20-525-6456
E-mail: hartl@science.uva.nl

[b] Dr. P. Rosa, Dr. L. Ricard, Dr. P. Le Floch
Laboratoire "Hétéroéléments et Coordination"
CNRS UMR 7653, École Polytechnique
91128 Palaiseau Cedex (France)

[c] Prof. M. J. Calhorda
ITQB, Av. da República, EAN, Apart. 127
2781-901 Oeiras (Portugal)

[d] Prof. M. J. Calhorda
Departamento de Química e Bioquímica, Faculdade de Ciências, Universidade de Lisboa
1749-016 Lisboa (Portugal)

  0947-6539/02/0807-1741 $ 20.00+.50/0

cally less demanding activation by light absorption or electron uptake/release in this case usually does not irreversibly destroy the low-nuclearity cluster core. On the other hand, it may trigger a significant change of bonding and physicochemical properties and reversible structural transformation. Fundamental to the success of the bottom-up approach towards larger assemblies containing switchable metal cluster moieties, are combined experimental and theoretical studies. The importance of the theoretical support for correct description of the bonding situation in relatively large, low-symmetry photo- and redox-responsive cluster compounds will be demonstrated in this work.

The intriguing photochemical and redox behavior of a series of triangular clusters $[Os_3(CO)_{10}(\alpha\text{-diimine})]$ (α-diimine = for example 2,2′-bipyridine (bpy), 2,2′-bipyrimidine (bpym), pyridine-2-carbaldehyde-*N*′-R-imine (R-PyCa; R = alkyl)) has been extensively investigated in the Amsterdam group in the last decade (Scheme 1).[1–4] Visible irradiation in

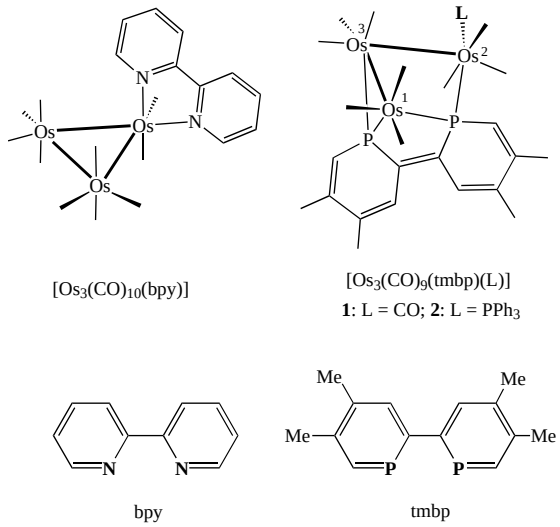

Scheme 1. Schematic molecular structures of the clusters $[Os_3(CO)_{10}(bpy)]$ and $[Os_3(CO)_9(tmbp)(L)]$ (**1**: L = CO; **2**: L = PPh_3), and of the ligands tmbp and bpy.

non- and weakly coordinating solvents like 2-chlorobutane, THF, or acetone leads to homolytic cleavage of an Os–Os(α-diimine) bond and reversible formation of short-lived biradical photoproducts $[(CO)_4Os^{\bullet}-Os(CO)_4-Os^{+}(CO)_2(\alpha\text{-diimine}^{\bullet-})]$.[1, 2] Electrochemical reduction of $[Os_3(CO)_{10}(\alpha\text{-diimine})]$ initially gives the radical anions $[Os_3(CO)_{10}(\alpha\text{-diimine}^{\bullet-})]$, which are thermally unstable and convert to various anionic open-triangle products in a series of chemical and electron-transfer steps.[3, 4] In both the biradical photoproducts and the radical anions there is an unpaired electron localized on the reducible α-diimine ligand. As a consequence, the electronic properties of the α-diimine play a major role in the photo- and electrochemistry of the clusters. Decreasing the energy of the lowest empty $\pi^*(\alpha\text{-diimine})$ orbital improves the ability of the α-diimine to accommodate the electron density, which increases the lifetime of the biradical photoproducts as well as the stability of the radical anions.

Closely related to the hitherto employed bidentate α-diimine ligands, in particular 2,2′-bipyridine (bpy), is the phosphorus derivative 4,4′,5,5′-tetramethyl-2,2′-biphosphinine (tmbp) (see Scheme 1). It was first synthesized in the early 1990s,[5] and since then its versatile coordination chemistry has been extensively explored.[6, 7] Compared with that of bpy, the π_1^*(tmbp) LUMO lies significantly lower in energy, as reflected, for example, in the strongly positively-shifted reduction potential ($E_{1/2}(tmbp^{0/-1}) = -1.85$ V and $E_{1/2}(bpy^{0/-1}) = -2.20$ V vs. SCE).[8] Other important differences are larger (d)M–P=C(π^*) overlap than that for (d)M–N=C(π^*), caused by the larger s-character of the phosphorus lone pair, and a partial positive charge on the P atom in the phosphinine heterocycle and a partial negative charge on nitrogen in pyridine.[7b] Owing to these factors, coordinated tmbp is a stronger π acceptor than bpy and better stabilizes low oxidation states of the metal in the M($\sigma P,\sigma P'$-tmbp) chelate ring in a variety of complexes, such as homoleptic $[Ni(tmbp)_2]^n$ (n = 0, −1),[9] $[M(tmbp)_3]$ (M = Group 4 metals,[10] W[11]) and $[M(tmbp)_2]^{2-}$.[12] In contrast, the rather limited σ-donor ability of neutral tmbp prevents, for example, the preparation of $[Ru^{II}(tmbp)_3]^{2+}$.[7]

The fairly different electronic properties of tmbp and bpy inspired us to attempt the synthesis of the cluster $[Os_3(CO)_{10}(\sigma P,\sigma P'\text{-tmbp})]$, so as to perform comparative spectroscopic, photochemical, and electrochemical studies. However, instead of the intended product, a structural isomer was obtained,[13] presenting the first example of a biphosphinine coordinated to three transition metal centers as a doubly bridging ligand (cluster **1** and and its PPh_3-derivative **2** in Scheme 1). To obtain a good insight into the unusual bonding properties of clusters **1** and **2**, a DFT[14] study, using the ADF program,[15] was performed. The computed models were based on the crystal structure of **1**, reported in a preceding communication,[13] and that of **2**, which is presented in this paper. The redox behavior of the two clusters was also investigated in detail and will be compared with that of $[Os_3(CO)_{10}(bpy)]$ and nonsubstituted $[Os_3(CO)_{12}]$.

Results and Discussion

Crystal structures of $[Os_3(CO)_9(tmbp)(L)]$ (L = CO (1), PPh_3 (2)): The CO-substituted derivative of **1**, the cluster $[Os_3(CO)_9(tmbp)(PPh_3)]$ (**2**), was prepared in high yield from **1** by an electrocatalytic substitution of CO by PPh_3. The details of this reaction and characterization of **2** will follow hereafter. We decided to study the bonding properties of both clusters to learn the influence of the additional Lewis base thereon. Careful analysis of X-ray structural data provides important information in this regard. Knowledge of the X-ray structure is also imperative for choosing a good model for density functional calculations, in particular for cluster **2**, which may exist in several possible isomeric forms. (The coordination site of PPh_3 could also be assigned by analysis of ^{31}P NMR data, see Experimental Section.)

The single-crystal X-ray studies of clusters **1**[13] and **2** (details in Experimental Section) revealed that the overall structures of these compounds are very close, both involving highly unusual coordination of tmbp (Figure 1, Table 1, see also Scheme 1).

  0947-6539/02/0807-1742 $ 20.00+.50/0 *Chem. Eur. J.* **2002**, *8*, No. 7

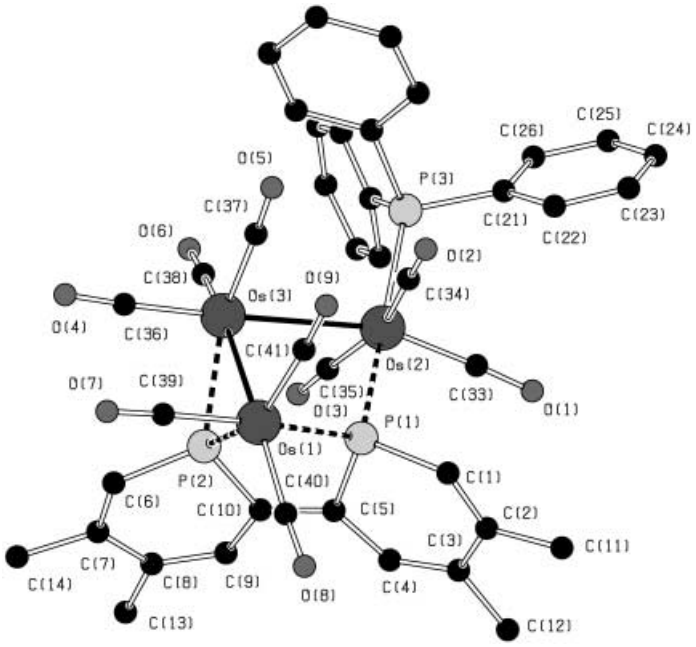

Figure 1. Crystal structure of the cluster $[Os_3(CO)_9(tmbp)(PPh_3)]$ (**2**).

Table 1. Selected bond lengths [Å] and bond angles [°] for cluster **2**, with standard deviations in parentheses.

Os1–Os3	2.8741(7)	C2–C3	1.466(8)
Os2–Os3	3.003(1)	C3–C4	1.361(8)
Os1–P1	2.418(2)	C4–C5	1.431(8)
Os1–P2	2.355(2)	C6–C7	1.344(8)
Os2–P1	2.428(2)	C7–C8	1.45(1)
Os2–P3	2.414(2)	C8–C9	1.36(1)
Os3–P2	2.378(2)	C9–C10	1.437(8)
P1–C1	1.789(6)	Os1–Os3–Os2	86.23(2)
P1–C5	1.823(6)	Os1–P1–Os2	112.00(6)
P2–C6	1.778(7)	Os1–P2–Os3	74.78(5)
P2–C10	1.803(6)	P1–Os1–P2	74.60(6)
C5–C10	1.372(8)	C1–P1–C5	101.8(3)
C1–C2	1.355(8)	C6–P2–C10	101.3(3)

Similar to the 4e⁻ donor 2,2′-bipyridine in $[Os_3(CO)_{10}(bpy)]$, the biphosphinine ligand is chelated at Os(1). At the same time, however, each tmbp phosphorus atom forms a bridge between Os(1) and one of the other two osmium centers. Cleavage of the Os(1)–Os(2) bond has opened the osmium triangle: Os(1)-Os(3)-Os(2) 85.93(2)° for cluster **1** and 86.23(2)° for cluster **2**. In both cases the tmbp ligand is strongly distorted and its aromaticity is lifted. In the majority of its mononuclear complexes tmbp displays a high degree of aromaticity; the phosphinine rings are perfectly coplanar, with intra-ring C–C bond lengths between 1.38 and 1.41 Å.[6, 7] In contrast, the C–C bond lengths in **1** and **2** range from 1.33/1.34 Å, typical for isolated C=C bonds, to 1.46/1.47 Å, close to the value for a single C–C bond (ca. 1.53 Å). Importantly, the inter-ring C–C bond is undoubtedly shorter for clusters **1** (1.41(2) Å) and **2** (1.372(8) Å), compared with the characteristic values for the nonreduced uncoordinated ligand (1.484(6) Å, *trans* isomer)[8] and for mononuclear complexes of tmbp (ca. 1.47 Å).[6, 7] Also the P–C bonds are rather long (1.78 Å (external), 1.81 Å (internal)) compared with P–C bond lengths for "aromatic" tmbp (1.72 Å (external), 1.74 Å (internal)).[6, 7] These data point to reduction of the tmbp ligand by intramolecular electron transfer from the triosmium core, a process that also causes the cleavage of the Os(1)–Os(2) bond. Recently, Le Floch and co-workers grew monocrystals of the radical anion and dianion of uncoordinated tmbp and succeeded in elucidating their crystal structures. Indeed, comparison of the structural data for tmbp in **1** and **2** (Figure 2D) with those for uncoordinated neutral tmbp[8] (Figure 2A), its radical anion,[9b] (Figure 2B) and dianion[16] (Figure 2C), convincingly demonstrates that the tmbp ligand can be considered as doubly reduced in both triosmium clusters.

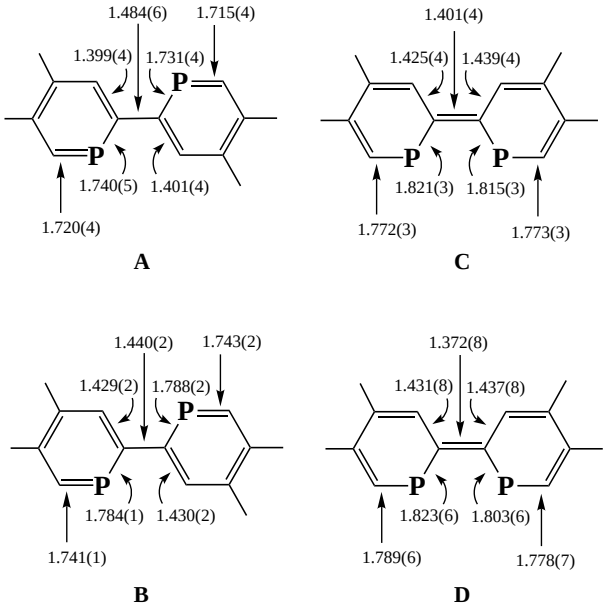

Figure 2. Schematic molecular structures with relevant bond lengths [Å] for neutral uncoordinated tmbp[8] (structure A), the corresponding radical anion[9b] (structure B) and dianion[16] (Na_2tmbp, structure C), and for tmbp coordinated in cluster **2** (structure D).

The close correspondence between the C–C and P–C distances in the tmbp coordinated in **2** and those in free $[tmbp]^{2-}$ is striking. In both cases the phosphinine rings are not coplanar. The lowest unoccupied π*(tmbp) orbital (LUMO) is antibonding with respect to the P–C bonds, and bonding with respect to the inter-ring C–C bond.[11] For this reason tmbp coordination at the triosmium core and the concomitant electron transfer to the LUMO of tmbp result in elongation of the P–C bonds and shortening of the inter-ring C–C distance. A similar situation applies for several transition metal complexes with negatively charged tmbp ligands, such as $[W(tmbp)_3]$, $[M(tmbp)_3]^{2-}$ (M = Zr, Hf, Ti), and $[Mn(CO)_3(tmbp)]^-$.[10, 11, 17, 18] The shorter inter-ring C–C distance in cluster **2** (1.372(8) Å, even slightly shorter than that in noncoordinate tmbp dianion[16], Figure 2) compared with **1** (1.41(2) Å, between the values for noncoordinate tmbp radical anion and dianion,[9b, 16] Figure 2) points to the positive influence of the donor PPh_3 ligand on the completion of the 2e⁻ oxidative "addition" of tmbp to the $\{Os_3(CO)_9(L)\}$ fragment.

Clusters **1** and **2** represent the first examples of coordinated tmbp in which each phosphorus atom forms a bridge between two metal centers. The bridging ability of the phosphorus atom in related ligands with a single phosphinine ring has already been reported in the literature. In the dimers $[M_2(cod)_2(niphos)]_2^{2+}$ (M = Ir, Rh; cod = 1,5-cyclooctadiene; niphos = 2-(2′-pyridyl)-4,5-dimethylphosphinine) the metal–metal bond is bridged by the phosphorus atoms of both phosphinine rings; however, the aromaticity of the phosphinine rings is preserved.[19] More interesting in this respect is the cluster $[Os_3(\mu\text{-}H)_2\{\mu^3\text{-}(t\text{-}Bu\text{-}C_5H_4P)\}(CO)_9]$, synthesized by Arce and co-workers (Figure 3).[20] The aromaticity of the

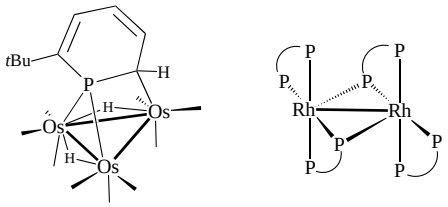

Figure 3. Examples of metal complexes with bridging (bi)phosphinine ligands. Left: $[Os_3(\mu\text{-}H)_2(\mu_3\text{-}(t\text{-}Bu\text{-}C_5H_4P))(CO)_9]$[20]; right: $[Rh(tmbp)_2]_2$.[7b]

phosphinine ligand in this cluster is completely disrupted by *ortho*-metalation, as indicated by the two localized C=C bonds in the phosphinine ring. Recently, the dimers $[Rh(tmbp)_2]_2$ (Figure 3)[7b], $[Ru(\eta^5\text{-}C_5Me_5)(tmbp)]_2$,[21] and $[Fe(tmbp)_2]_2^{2-}$[7b] were synthesized by Le Floch and co-workers. In these dimers, two tmbp ligands bridge two metal centers through one of their phosphorus atoms. Only in the case of $[Fe(tmbp)_2]_2^{2-}$ the bridging phosphinine rings are not aromatic, indicating that the negative charge is largely localized on the bridging tmbp ligands (see below). In general, phosphinine rings such as in tmbp appear to favor a bridging coordination mode in polynuclear transition metal complexes.[7b]

The structures of clusters **1** and **2** are reminiscent of that of $[Os_3(CO)_{10}(ER)_2]$ (E = Se, R = Me, Ph; E = Te, R = Ph), in which both ER^- groups connect two osmium centers and, again, one of the bridged metal–metal bonds is broken (see Figure 4).[22, 23] According to cluster electron-counting rules, clusters **1**, **2**, $[Os_3(CO)_{10}(ER)_2]$, and related compounds with only two metal–metal bonds are considered to be 50e⁻ clusters.[24] Each phosphorus atom of the nonreduced aromatic biphosphinine is a 2e⁻ donor. Contrary to this, the crystal structures show that the P atoms in **1** and **2** are formally sp^3-hybridized and therefore equivalent to the phosphido ligands: PR_2^- as 4e⁻ donor or PR_2 as 3e⁻ donor, depending on the counting method. Taking into account the ′localized′ phosphinine ring C–C and C=C bonds and the short inter-ring C=C bond, the tmbp ligand in **1** and **2** is indeed formally best described as an 8e⁻ donor in $\{Os_3(CO)_9(L)\}^{2+}/[tmbp]^{2-}$ or 6e⁻ donor in $\{Os_3(CO)_9(L)\}$/tmbp.

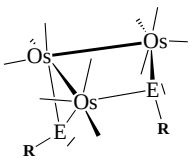

Figure 4. Schematic structure of the 50e⁻ cluster $[Os_3(CO)_{10}(\mu\text{-}ER)_2]$ (E = Se, Te; R = Me, Ph) with only two metal–metal bonds.[22, 23]

Density functional study of $[Os_3(CO)_9(2,2'\text{-biphosphinine})(L)]$, L = CO, PH_3: Density functional theoretical (DFT[14]) calculations were performed with the ADF program[15] (see details in Experimental Section) in order to obtain more insight into the electronic structures of clusters **1** and **2**, and to understand the preferential formation of these structural isomers. The cluster $[Os_3(CO)_{10}(bp)]$ (bp = 2,2′-biphosphinine), **1A**, was taken as a model for **1**, with the methyl groups in the tmbp ligand replaced by hydrogen atoms. The optimized geometry of **1A** (Figure 5, left) is in good

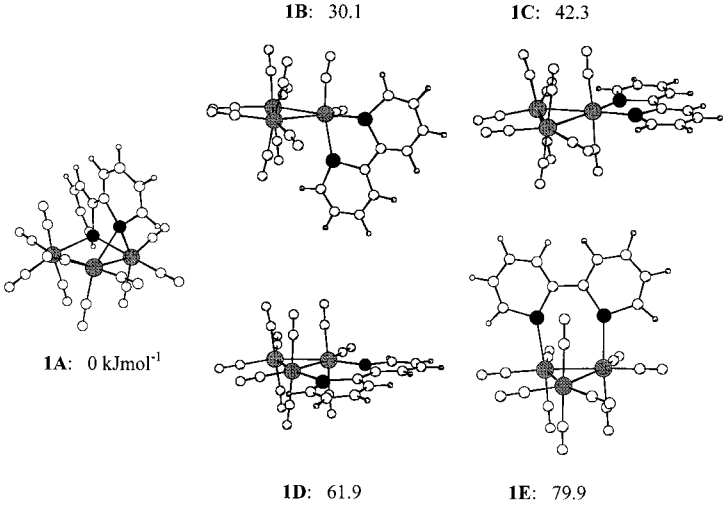

Figure 5. Optimized geometries and relative energies (kJ mol⁻¹) of the model cluster $[Os_3(CO)_{10}(bp)]$ **1A** and its isomers **1B–E**.

agreement with the experimental structure of **1**, although the calculated Os–Os, Os–P, and P–C bond lengths are slightly larger than the experimental values. Indeed, the Os–Os distances are calculated to be 4.137, 3.009, and 3.092 Å, while the experimental ones are 3.982, 2.886, and 2.957 Å, respectively. The four Os–P bonds (2.477, 2.536, 2.426 and 2.485 Å) are also longer than the corresponding experimental distances of 2.395, 2.441, 2.351, and 2.376 Å, respectively, but the same trends are observed. This difference appears to be a general result of DFT calculations and was also observed for the related complexes $[Os_3(CO)_{12}]$,[25] $[Os_3(CO)_{10}(\alpha\text{-diimine})]$,[26] and $[W(tmbp)_3]$[11]. In the optimized geometry of $[Os_3(CO)_{10}(bp)]$, however, the alternation of the C–C and C=C bonds in the biphosphinine rings is well reproduced.

The related $[Os_3(CO)_{10}(bpy)]$ cluster served as the basis for modelling other coordination geometries, namely the usually most stable axial isomer **1B**,[26] the equatorial isomer **1C**, and two isomers containing bridging (instead of chelating) bp, in the equatorial Os_3 plane **1D**, or in the plane perpendicular to it **1E**. Figure 5 shows **1A** together with these structural isomers, **1B–E**, and the calculated relative energies (kJ mol⁻¹).

Cluster **1** was synthesized with the intention of preparing the structural equivalent of $[Os_3(CO)_{10}(bpy)]$, with tmbp chelated at a single osmium center, but the theoretical calculations show isomer **1A** to be more stable by 30 kJ mol⁻¹ than isomer **1B**, the structural equivalent of the observed isomer of $[Os_3(CO)_{10}(bpy)]$. It cannot be excluded, however,

0947-6539/02/0807-1744 $ 20.00+.50/0 *Chem. Eur. J.* **2002**, *8*, No. 7

that **1B** is the kinetic reaction product, rapidly isomerising to **1A**. No temperature-dependent investigations have been performed so far in this regard. Isomer **1B**, with one phosphorus axial and the other one equatorial, is in turn more stable than isomer **1C** with both phosphorus atoms bound equatorially to the same osmium center. This trend has also been found for the corresponding structures of $[Os_3(CO)_{10}(bpy)]$.[26] The isomers **1D** and **1E**, with P atoms bound to different metals, are highest in energy.

The reasons underlying the preference for geometry **1A** observed in cluster **1** will be analyzed on the basis of the bond energy decomposition scheme, taking for comparison the second most likely isomer, **1B**, which is formed when nitrogen donor ligands are considered. According to this decomposition scheme, the bonding energy ΔE_{tot} is the sum of two terms, $\Delta E_{prep} + \Delta E_{int}$. ΔE_{prep} is the energy required to convert the separate fragments in their equilibrium geometry into fragments having the same geometry as in the molecule, while ΔE_{int} represents the interaction energy between the prepared fragments. ΔE_{int} can be further decomposed into three terms, namely $\Delta E_{int} = \Delta E_{Pauli} + \Delta E_{el} + \Delta E_{oi}$.[27] These terms correspond to the Pauli repulsion between occupied orbitals of the fragments (ΔE_{Pauli}) and the electrostatic interaction between the fragments (ΔE_{el}). The term ΔE_{oi} represents the two-electron stabilizing interactions between occupied levels of one fragment and filled levels of the other. ΔE_{oi} can be decomposed according to the number of irreducible representations, but in the absence of symmetry as in **1A** and **1B**, there is only one term $\Delta E_{oi}(a')$. The bond energy terms calculated for the two isomers **1A** and **1B**, when they are decomposed into fragments $\{Os_3(CO)_{10}\}^{2+}$ and bp^{2-}, and $\{Os_3(CO)_{10}\}$ and bp, respectively, are given in Table 2.

Table 2. Bonding energy decomposition for the two isomers **1A** and **1B** of the model cluster $[Os_3(CO)_{10}(bp)]$.

Isomer	**1A**	**1B**
fragments	$\{Os_3(CO)_{10}\}^{2+}$ and bp^{2-}	$\{Os_3(CO)_{10}\}$ and bp
ΔE_{Pauli}	363.7	256.4
ΔE_{el}	111.9	– 198.4
ΔE_{oi} (a′)	– 1484.3	– 149.1
$\Delta E_{prep}(1)$[a]	416.1	4.0
$\Delta E_{prep}(2)$[b]	32.4	24.2
ΔE_{tot}	*– 560.2*	*– 62.9*

[a] $\Delta E_{prep}(1)$ refers to the preparation energy of fragment 1, that is $\{Os_3(CO)_{10}\}^{2+}$ or $\{Os_3(CO)_{10}\}$ in **1A** or **1B**, respectively. [b] $\Delta E_{prep}(2)$ refers to the preparation energy of fragment 2, that is bp^{2-} or bp in **1A** or **1B**, respectively.

The term that decides about the higher stability of **1A** is ΔE_{oi}, showing that very strong covalent bonds are formed between the two fragments for this isomer. The price to pay is also clear. There is a very high preparation energy, indicating that the two fragments, and in particular the biphosphinine fragment, must change their geometry considerably in order to produce the cluster. Conversely, for the other isomer **1B**, weaker bonds are formed, but the fragments in their equilibrium geometry only need a small reorganization (In other words, there might be significant activation energy barrier when proceeding from the yet undetected kinetic isomer $[Os_3(CO)_{10}(\sigma P,\sigma P'\text{-tmbp})]$ to cluster **1**; again, temperature-dependent investigation of the synthesis is demanded). In the case of **1A**, the formally dicationic triosmium cluster core binds the dianionic bp ligand, with the formation of four Os–P bonds, as discussed on purely structural grounds above. In the coordinated ligand, two isolated P^- donors can be envisaged, which form four bonds (P–Os and P–C) each. The remaining carbon atoms in the ring form alternating C=C and C–C bonds (see Figure 2, right side). This alternative bonding mode is clearly more favorable for P than for N heteroatoms and can be traced to the smaller tendency to engage in P=C bond formation, as overlap between the P 3p and C 2p orbitals is reduced, a feature previously observed in simpler molecules such as pyrrole and phosphole.[28]

The composition of the frontier orbitals for model **1A** is given in Table 3 and the corresponding three-dimensional pictures in Figure 6. In contrast to what had been previously calculated for related α-diimine clusters,[26] not only the LUMO, but also the HOMO possesses predominant biphos-

Table 3. Energies and composition of the frontier orbitals of $[Os_3(CO)_{10}(bp)]$, **1A**, with the optimized structure.

MO	*E* [eV]	Composition [%]				
		Os1	Os2	Os3	CO	bp
107a	– 2.89	1.1	3.2	16.4	53.1	15.6
106a	– 2.98	1.4	2.9	1.7	23.7	66.0
105a	– 3.21	2.1	4.5	0.5	71.0	18.8
104a (LUMO)	*– 4.11*	*4.7*	*4.0*	*4.1*	*6.5*	*72.6 (π_2*)*
103a (HOMO)	*– 5.46*	*0.4*	*3.1*	*7.4*	*6.2*	*74.3 (π_1*)*
102a	– 5.89	27.0	4.6	26.5	24.0	8.0
101a	– 6.16	10.9	24.2	24.0	26.1	5.0
100a	– 6.61	3.2	0.8	51.1	16.6	22.7
99a	– 6.77	41.5	4.3	18.6	5.8	23.5
98a	– 6.79	29.7	6.3	32.6	2.4	22.4

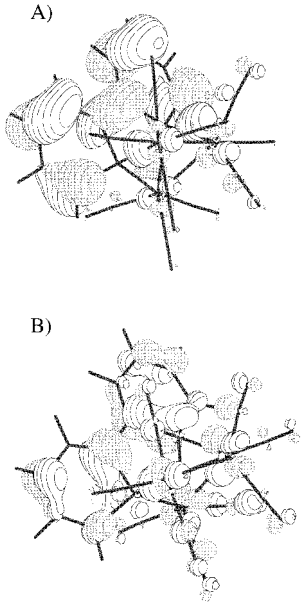

Figure 6. Three-dimensional representations of the frontier molecular orbitals of the model cluster $[Os_3(CO)_{10}(bp)]$, **1A**, showing the strong contribution of the bp ligand: A) the 103a HOMO; B) the 104a LUMO. See also Table 3.

phinine character, with contributions of two different π*(tmbp) orbitals. This result indicates that about two electrons were transferred from the cluster core to the biphosphinine ligand upon its binding, with consequent cleavage of one Os–Os bond, as could already be inferred from the preceding X-ray structural data.

In the substituted model cluster $[Os_3(CO)_9(PH_3)(bp)]$ (**2A**) the characters and relative energetic positions of the 103a HOMO and 101a LUMO remain nearly unchanged compared with **1A** (Table 4). Coordination of the phosphane ligand mainly affects the lower-lying HOMO-1 and HOMO-2,

Table 4. Energies and composition of the frontier orbitals of $[Os_3(CO)_9(PH_3)(bp)]$, **2A**, with the optimized structure.

MO	E [eV]	Composition [%]					
		Os1	Os2	Os3	CO	bp	PH_3
106a	−2.64	0.9	3.5	5.3	47.1	29.0	1.8
105a	−2.73	0.9	3.9	3.4	13.9	67.8	3.5
104a	−2.92	0.9	4.5	0.1	77.0	10.2	0.3
103a (LUMO)	*−3.92*	*2.3*	*5.3*	*2.4*	*9.5*	*68.2 (π_2*)*	*3.2*
102a (HOMO)	*−5.24*	*0.3*	*2.4*	*3.2*	*9.8*	*69.7 (π_1*)*	*6.5*
101a	−5.69	14.8	14.5	13.1	22.3	21.7	2.7
100a	−5.80	8.4	19.4	17.8	22.3	16.3	2.6
99a	−6.41	2.8	3.2	9.1	22.5	49.2	6.4
98a	−6.51	25.5	8.1	11.7	15.8	28.2	2.5
97a	−6.54	31.8	11.3	15.0	9.9	22.1	3.4

causing their more regular delocalization over the cluster core, with apparently increased biphosphinine contribution.

Time-dependent DFT calculations[29] were performed on the models **1A** and **2A** in order to reproduce and assign the experimental electronic absorption spectra for **1** and **2**, respectively. Several different conditions were tested, but even the best results still display a significant shift of the calculated transitions to lower energy (Figure 7). Besides the

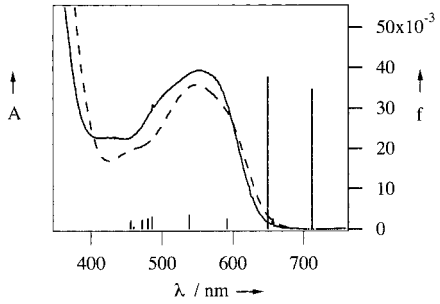

Figure 7. UV/Vis absorption spectra of **1** (solid line) and **2** (dashed line) in THF. The vertical bars represent absorption maxima of the visible electronic transitions calculated for model cluster **1A** by the time-dependent DFT; their relative intensities are given by the calculated oscillator strengths (f_{calc}).

problem of the significant spin-orbit coupling in the case of the heavy Os atoms, there is no optimization of excited states in the TD DFT calculations, which may also add to the discrepancies. The most satisfactory data presented in Table 5 (for **1A**) and Table 6 (for **2A**) have been obtained using the "zeroth order relativistic approximation" (ZORA)[30] formalism of ADF-1999 methodology for taking into account relativistic corrections.

Table 5. The calculated energies (E), absorption maxima (λ_{max}), oscillator strengths (f_{calc}), and assignments of the visible electronic transitions of $[Os_3(CO)_{10}(bp)]$ (**1A**) with the optimized structure.

No.	E [eV]	λ_{max} [nm]	f_{calc}	Nature	Contribution [%]
1	1.7406	712.3	3.48×10^{-2}	H → L	65
				H-1 → L	31
2	1.9088	649.5	3.77×10^{-2}	H-1 → L	67
				H → L	29
3	2.0956	591.6	2.60×10^{-3}	H-2 → L	98
4	2.3036	538.2	3.60×10^{-3}	H → L + 1	98
5	2.5523	485.8	3.17×10^{-3}	H → L + 2	66
				H-3 → L	24
6	2.5829	480.0	2.71×10^{-3}	H-3 → L	58
				H → L + 3	28
7	2.6292	471.6	2.28×10^{-3}	H → L + 3	62
8	2.6952	460.0	6.94×10^{-4}		
9	2.6964	459.8	5.65×10^{-4}		
10	2.7222	455.5	2.24×10^{-3}	H-5 → L	89

Table 6. The calculated energies (E), absorption maxima (λ_{max}), oscillator strengths (f_{calc}), and assignments of the visible electronic transitions of $[Os_3(CO)_9(PH_3)(bp)]$ (**2A**) with the optimized structure.

No.	E [eV]	λ_{max} [nm]	f_{calc}	Nature	Contribution [%]
1	1.7298	716.8	3.95×10^{-2}	H → L	69
				H-1 → L	26
2	1.8650	664.8	2.93×10^{-2}	H-1 → L	72
				H → L	25
3	2.0956	641.9	2.92×10^{-3}	H-2 → L	97
4	2.3400	529.9	9.23×10^{-4}	H → L + 1	99
5	2.5550	485.8	4.97×10^{-3}	H-3 → L	75
				H → L + 2	22
6	2.5879	479.1	2.04×10^{-3}	H → L + 2	43
				H → L + 3	31
7	2.6252	472.3	4.05×10^{-4}	H-4 → L	88
8	2.6491	468.0	1.56×10^{-3}	H → L + 3	44
				H-5 → L	41
9	2.6817	462.3	1.78×10^{-3}	H-5 → L	44
10	2.7547	450.1	4.18×10^{-3}	H → L + 4	91

The UV/Vis absorption spectra of **1** and **2** display an intense and broad absorption band at about 550 nm, which is shown to consist of two well-separated electronic transitions of comparable oscillator strengths (Figure 7). The lowest-energy one is essentially the HOMO-to-LUMO transition (65–70%) mixed with the (HOMO-1)-to-LUMO (30–25%) transition, other contributions being negligible. The second absorption band belongs to a transition that possesses a complementary character, the (HOMO-1)-to-LUMO excitation being more important (65–70%) than the HOMO-to-LUMO one (30–25%). As both the HOMO and the LUMO of the model clusters **1A** and **2A** are strongly localized on the 2,2′-biphosphinine ligand, it can be said that the lowest-energy electronic transition possesses a predominant tmbp-localized intraligand character. This assignment is in contrast to the corresponding solvatochromic transition of $[Os_3(CO)_{10}(bpy)]$, which has been classified as charge transfer from the cluster core to the lowest π*(bpy) orbital.[26, 31] The difference in the character of the lowest-energy electronic transitions explains the previously reported absence of solvatochromism for the corresponding visible absorption band of **1**, and the lacking photoreactivity.[13] The same behavior and conclusions essentially apply for **2**. Even though the calculated energies for the

0947-6539/02/0807-1746 $ 20.00+.50/0 *Chem. Eur. J.* **2002**, *8*, No. 7

visible electronic transitions deviate from the experimental values, the trends are correct. Thus, in accordance with the TD-DFT data for **1A** and **2A** (Table 5, Table 6), the lowest-lying transition shifts slightly to lower energy on going from **1** to **2** (Figure 7) and its intensity somewhat drops.

The two higher lying visible electronic transitions possess a predominant (HOMO-1)-to-LUMO and exclusive (HOMO-2)-to-LUMO character, respectively. The former transition is again intense while the calculated intensity of the latter transition is significantly lower. On grounds of the DFT data, these transitions are expected to possess more pronounced cluster core to tmbp charge transfer character. The latter one corresponds in the UV/Vis spectra of **1** to the shoulder at ca 550 nm (in THF, Figure 7), probably partly overlapping with a close-lying band caused by the HOMO-to-(LUMO+1) transition of similar intensity. Indeed, characteristic for this kind of transition, the shoulder shifts to lower energy in less polar hexane relative to the lowest energy transition, and the composed absorption band becomes symmetric.

A similar shift occurs on the substitution of the CO in **1** by PPh_3, as evidenced by the UV/Vis spectrum of **2** (Figure 7). In this case the shift relates to the smaller energetic separation between the HOMO-2 and LUMO, as calculated for the model **2A** (Table 6).

In view of the above discussion, the weak band/shoulder at about 420–460 nm in the UV/Vis spectra of **1** and **2** is assigned to the group of low-intensity transitions labelled as numbers 5–10 in Tables 5 and 6 (Figure 7).

Redox behavior of clusters 1 and 2: The redox potentials and IR ν(CO) wavenumbers of cluster **1**, the PPh_3 derivative **2**, and their reduction products are summarized in Table 7 and Table 8, respectively. All (spectro)electrochemical experiments were performed in THF, unless stated otherwise.

Table 7. Redox potentials of clusters **1** and **2** and their reduction products.[a]

Cluster	$E_c(R_1)$	$\Delta E_p(R_1/O_1)$	$E_c(R_2)$	$E_a(O_2(\mathbf{B}))$	$E_a(O_2(\mathbf{B}'))$
1	−1.75 (irr)			−1.53	−1.27
1[b]	−1.80	125 (120)	−2.19	−1.48	−1.23
1[c]	−1.80 (rev)	105 (100)	−2.18	−1.49[d]	−1.27[d]
2	−1.93 (irr)			−1.55	−1.29
2[e]	−1.92 (rev)	80 (105)	−2.29	−1.51[d]	−1.26[d]

[a] Conditions and definitions: 5×10^{-4} M solutions in THF (containing 10^{-1} M Bu_4NPF_6) at $T=293$ K, unless stated otherwise; Pt disk electrode; $\nu=100$ mV s^{-1}; redox potentials given in V vs. $E_{1/2}(Fc/Fc^+)$: $E_c(R_1)$, cathodic peak potential for reduction of parent cluster, $E_c(R_2)$, cathodic peak potential for reduction of the corresponding radical anion; E_a, anodic peak potential for oxidation of the reduction products; ΔE_p, peak separation for a redox couple (compared with $\Delta E_p(Fc/Fc^+)$ in brackets). [b] $\nu=20$ V s^{-1}. [c] $T=244$ K. [d] Both anodic peaks are associated with the reduction of the radical anion at $E_c(R_2)$. [e] $T=252$ K.

Cyclic voltammetry: At room temperature, cluster **1** undergoes chemically irreversible reduction (cathodic peak R_1(**1**); Figure 8A). The anodic peak O_2(**B**) on the reverse scan is associated with this cathodic process and corresponds to oxidation of a secondary reduction product, **B**. At $\nu=20$ mV s^{-1} no other anodic peaks are observed, but at higher scan rates ($\nu=100$ mV s^{-1}) a second anodic peak O_2(**B′**) starts to grow in at the expense of O_2(**B**). At $\nu=10$ V s^{-1} reoxidation

Table 8. IR CO-stretching wavenumbers of clusters **1** and **2** and their reduction products.

Cluster	ν(CO) [cm^{-1}]
1[a]	2104(m), 2052(s), 2021(sh), 2018(vs), 1982(m), 1966(m), 1941(m)
1[b]	2109(m), 2053(s), 2023(sh), 2019(vs), 2007(sh), 1983(m), 1965(m), 1938(m)
1$^{\bullet-}$[b]	2082(m), 2020(vs), 2006(s), 1987(s), 1977(sh), 1947(m), 1932(m), 1905(m)
2[a]	2061(m), 2036(s), 2003(vs), 1988(s), 1970(m), 1958(m), 1932(m)
B[a,c]	2009(m), 1952(s), 1947(sh), 1929(m), 1876(m), 1858(sh), 1716(sh), 1693(w)
C[a,c]	2033(m), 2006(m), 1981(s), 1952(m), 1922(sh), 1912(m)
C[d]	2060(w), 2050(w), 2028(m), 1983(s), 1953(m), 1945(sh), 1916(m)
C[a,e]	2050(w), 2033(w), 2022(m), 2007(w), 1979(s), 1954(m), 1922(sh), 1911(m)

[a] In THF at 293 K. [b] In situ reduction in butyronitrile at 213 K within an IR OTTLE cell[57]. [c] In situ reduction at room temperature within an IR OTTLE cell[56]. [d] Chemical reduction with [Fe^I(η^5-C_5H_5)(η^6-C_6Me_6)], performed in DME. [e] Chemical reduction with 1% Na/Hg.

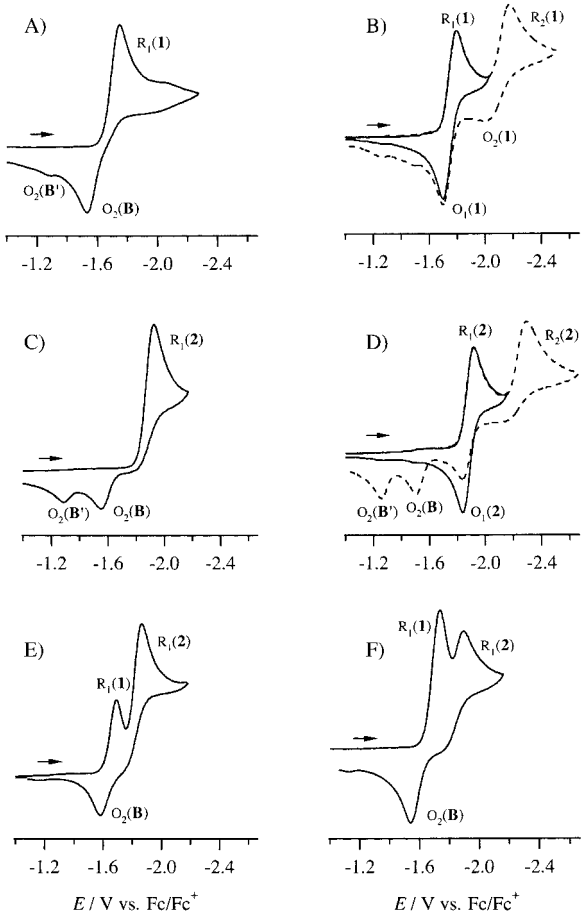

Figure 8. Cyclic voltammograms of clusters **1** and **2** in THF. Conditions: A. **1**, $\nu=100$ mV s^{-1}, 293 K; B. **1**, $\nu=100$ mV s^{-1}, 244 K; C. **2**, $\nu=100$ mV s^{-1}, 293 K; D. **2**, $\nu=100$ mV s^{-1}, 252 K; E. **1** in the presence of excess PPh_3, $\nu=20$ mV s^{-1}, 293 K; F. **1** in the presence of excess PPh_3, $\nu=100$ mV s^{-1}, 293 K.

of the primary radical anion **1**$^{\bullet-}$ becomes observable (anodic peak O_1(**1**)), together with its reduction to the dianion **1**$^{2-}$ at $E_c(R_2(\mathbf{1}))$. At $\nu=50$ V s^{-1} the formation of **1**$^{\bullet-}$ is almost completely chemically reversible. The one-electron reduction of **1** becomes fully reversible at lower temperatures ($T\leq243$ K; $\nu=100$ mV s^{-1}; Figure 8B). The subsequent reduction of the radical anion **1**$^{\bullet-}$ to **1**$^{2-}$ remains irreversible even at 213 K. At this temperature **1**$^{2-}$ decomposes to the same product **B′** that is formed upon reduction of **1** at R_1(**1**) at room temperature, as testified by the anodic peak O_2(**B′**) at 213 K. At higher temperatures also O_2(**B**) is observed. Summarizing,

the transient species **B′** (only observable at low temperatures or high scan rates) is formed from **1** in an overall two-electron process[32] and rapidly reacts further to give the more stable product **B**, which could be identified as $[Os_3(CO)_9(tmbp)]^{2-}$ (vide infra). At low temperatures an EEC path is followed, according to which two cathodic steps (E) (the stepwise formation of $\mathbf{1}^{\bullet-}$ and $\mathbf{1}^{2-}$) are first needed to induce a chemical reaction (C) to produce **B′**. At room temperature and/or low scan rates, the sequence changes to ECE, as the radical anion $\mathbf{1}^{\bullet-}$ readily undergoes a chemical reaction and its product is directly reduced at the cathodic potential $R_1(\mathbf{1})$ to give **B′** and **B**.

The redox behavior of **2** proved to be very similar to that of **1** (Figure 8C, D), in agreement with their similar structure and bonding properties. The reduction of **2** at $R_1(\mathbf{2})$ at room temperature is chemically irreversible and is shifted negatively ($\Delta E_{1/2} = 130$ mV; see Table 7) compared with that of **1**, as expected for the substitution of a π-acceptor CO ligand by more basic PPh_3. At sufficiently low temperatures ($T \leq 253$ K, $\nu = 100\ mV\,s^{-1}$), the initial one-electron reduction that produces the radical anion $\mathbf{2}^{\bullet-}$ again becomes fully reversible on the time scale of cyclic voltammetry. Upon scan reversal beyond $E_c(R_1(\mathbf{2}))$ at room temperature, the anodic peaks $O_2(\mathbf{B})$ and $O_2(\mathbf{B'})$ are observed at exactly the same potentials, as they were for **1**. This result implies that the reduction of **1** and **2** yields the same products **B** and **B′**.

IR spectroelectrochemistry: To further characterize the reduction products formed, the reduction pathways of **1** and **2** were studied by IR spectroelectrochemistry and thin-layer cyclic voltammetry on the same time scale (defined by $\nu = 5\ mV\,s^{-1}$).

At temperatures below 243 K, the primary reduction product, the radical anion $\mathbf{1}^{\bullet-}$, becomes stable on the time scale of cyclic voltammetry ($\nu \geq 100\ mV\,s^{-1}$). Its IR spectrum could be recorded in butyronitrile at 213 K (see Figure 9). As

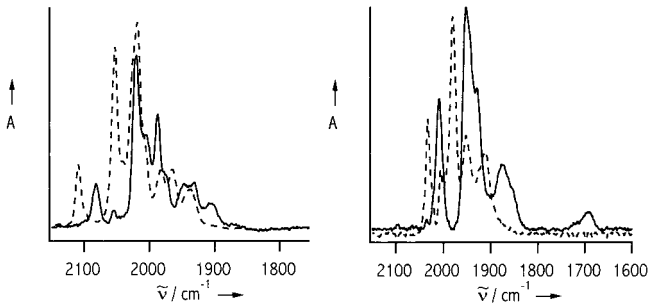

Figure 9. IR spectra of cluster **1** and its reduction products generated in situ within an IR OTTLE cell. Left: cluster **1** (dashed line) and the corresponding radical anion $\mathbf{1}^{\bullet-}$ (solid line) in butyronitrile at 213 K. Right: reduction products $\mathbf{B} = [Os_3(CO)_9(tmbp)]^{2-}$ (solid line) and unassigned **C** (dashed line) in THF at room temperature.

expected, the ν(CO) pattern of $\mathbf{1}^{\bullet-}$ is nearly the same as that of **1**, with the ν(CO) bands shifted to smaller wavenumbers by 30–35 cm^{-1}, and with the strongest band (at 2019 cm^{-1} for **1**) split into two bands of lower intensities. Therefore, the molecular structure of $\mathbf{1}^{\bullet-}$ will strongly resemble that of the parent cluster.

According to the recorded cyclic voltammograms, the same secondary reduction product **B** is formed for clusters **1** and **2** (vide supra). Indeed, the common formation of **B** upon reduction of both clusters at room temperature was also proved by IR spectroelectrochemistry (see Figure 9). For **1**, an additional side product, denoted as **C**, is formed (Table 8). Reoxidation of product **B** at $E_a(O_2(\mathbf{B}))$ (Table 7) results in regeneration of **1** and **2**, respectively, although, for the former cluster the amount of **C** also increased simultaneously.

The sole difference between **1** and **2** is the substitution of a carbonyl ligand by PPh_3, which leads to a changed IR ν(CO) pattern. Hence, only the dissociation of the two-electron donors CO and PPh_3 can explain the formation of the same product upon reduction of **1** and **2**, respectively. We therefore propose that **B** is the CO/PPh_3-loss product $[Os_3(CO)_9(tmbp)]^{2-}$ (see Scheme 2). The dianionic nature of **B** is

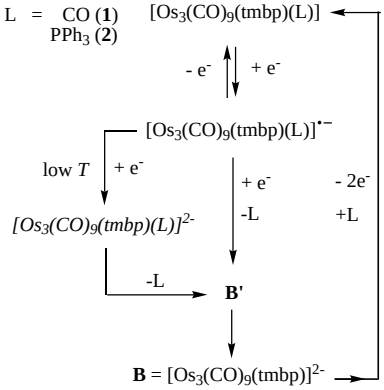

Scheme 2. Reduction pathways for the clusters $[Os_3(CO)_9(tmbp)(L)]$ (L = CO (**1**), PPh_3 (**2**)).

in agreement with the cyclic voltammetric data (vide supra). Additional support is given by the IR spectrum of **B**. Its ν(CO) bands are generally shifted to lower wavenumbers by nearly 100 cm^{-1} compared with those of **1**, and two weak bands at 1716 and 1693 cm^{-1} point to the presence of bridging CO ligands. Such a large shift of the ν(CO) is typical for two-electron-reduced clusters with the negative charge significantly localized on the triosmium/carbonyl core.[4, 33, 34]

To extend characterization of the reduction products **B** and **C**, by NMR spectroscopy for example, their preparation was attempted by chemical reduction of cluster **1** at room temperature, by reduction of **1** in THF with 1% Na/Hg, and by addition of exactly two equivalents of $[Fe^{I}(\eta^5\text{-}C_5H_5)(\eta^6\text{-}C_6Me_6)]$ ($E_{1/2}(Fe^{I/II}) = -1.99$ V vs. Fc/Fc^+) to a solution of **1** in DME. Unfortunately, both attempts were not successful and only provided the slowly decomposing reduction product **C** (see above and Table 8), accompanied by some minor side-products.

*Electrocatalytic CO substitution reaction of **1***: Electrocatalytic substitution of CO by more electron-releasing ligands is a versatile method to synthesize substituted metal carbonyl complexes.[35] It was therefore also attempted in the case of **1** with the electron deficient cluster core. The cyclic voltammograms of **1** in the presence of an excess of PPh_3 at various

  0947-6539/02/0807-1748 $ 20.00+.50/0 *Chem. Eur. J.* **2002**, *8*, No. 7

temperatures and scan rates are presented in Figure 8E, F. The cyclic voltammogram recorded at room temperature and $\nu = 100\ mV\,s^{-1}$ shows a decrease of the cathodic peak current at $E_c(R_1(\mathbf{1}))$ and the appearance of a new cathodic peak $R_1(\mathbf{2})$ at slightly more negative potential ($E_c(R_1(\mathbf{2})) = -1.90$ V vs. Fc/Fc^+). At lower scan rate ($\nu = 20\ mV\,s^{-1}$) the current of the latter cathodic peak increases at the expense of that of $R_1(\mathbf{1})$. The new cathodic peak $R_1(\mathbf{2})$ arises because of the reduction of the neutral cluster $[Os_3(CO)_9(PPh_3)(tmbp)]$ (**2**) (vide supra) produced by the reaction of the radical anion $\mathbf{1}^{\bullet-}$ with PPh_3 (Scheme 3).

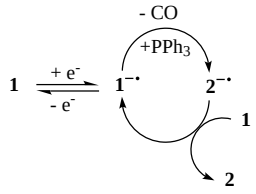

Scheme 3. Electrocatalytic substitution of CO by PPh_3 in cluster **1**.

The increased $R_1(\mathbf{2})$ and decreased $R_1(\mathbf{1})$ currents at lower scan rates are indicative of an electrocatalytic step, since **2** then builds up at the cathodic surface at higher concentrations. The electrocatalytic formation of the substitution product can eventually be so fast that the initial redox process of the parent complex is hardly observable at slow voltammetric scans.[36] Continued cyclic voltammetric studies showed that other PR_3 ligands (R = ethyl, cyclohexyl, OPh) also undergo the electrocatalytic substitution reaction with **1**.[37] It is noteworthy that CO substitution was not observed in the presence of other substrates such as $AsPh_3$, pyridine, 1-octene, or diphenylacetylene.

As decribed above, the phosphane-substituted cluster $[Os_3(CO)_9(PPh_3)(tmbp)]$ (**2**) could also be synthesized on a preparative scale in high yield. Cluster **1** reacts instantaneously in THF at room temperature with a catalytic amount (5%) of sodium biphenyl ketyl in the presence of three equivalents of PPh_3 to give **2** as the single product, hence providing additional evidence for the mechanism given in Scheme 2.

*Comments on the redox behavior of cluster **1***: The DFT calculations predict that the LUMO of **1** is predominantly localized on tmbp. For this reason, it is assumed that in the radical anion $\mathbf{1}^{\bullet-}$ the unpaired electron resides on this ligand. Comparison of the reduction potentials of uncoordinated aromatic tmbp and some of its metal complexes with those of their bpy or 4,4′-dimethyl-2,2′-bipyridine (dmb) derivatives shows that the former complexes are systematically reduced more positively by 300–350 mV, (e.g., $E_{1/2}(tmbp^{0/-1}) = -1.85$ V, $E_{1/2}(dmb^{0/-1}) = -2.16$ V vs. SCE;[8] $E_{1/2}([Ni(tmbp)_2]^{0/-1}) = -1.64$ V, $E_{1/2}([Ni(bpy)_2]^{0/-1}) = -1.97$ V vs. SCE).[9] In the case of **1**, the reduction potential lies much closer to that of $[Os_3(CO)_{10}(dmb)]$[38]: $E_{1/2}([Os_3(CO)_{10}(tmbp)]^{0/-1}) = -1.80$ V (244 K) and $E_{1/2}([Os_3(CO)_{10}(dmb)]^{0/-1}) = -1.89$ V (213 K) vs Fc/Fc^+. These data reflect the different coordination mode and the reduced state of tmbp in **1**. For unsubstituted $[Os_3(CO)_{12}]$ the corresponding radical anion is too short-lived to be detected, because of its fast follow-up chemical reactions.[39] By contrast, $\mathbf{1}^{\bullet-}$ is sufficiently stable for observation with both cyclic voltammetry and IR spectroelectrochemistry at low temperatures. Two factors are responsible for the increased stability of the radical anion. First, the one-electron reduction is not localized on the cluster core, but on the redox-active tmbp ligand, and second, tmbp spans the triosmium core. Remarkably stable radical anions were also observed for the clusters $[HOs_3(CO)_9(o\text{-}L)]$, in which the redox-active ligand *o*-L is an *ortho*-metalated α-diimine bridging an Os–Os bond.[4]

At room temperature, the radical anion $\mathbf{1}^{\bullet-}$ is not stable and undergoes a chemical reaction and a second electron transfer step, ultimately producing the CO-loss product $[Os_3(CO)_9(tmbp)]^{2-}$. Such replacement of a two-electron donor ligand by two external electrons occurs frequently in cluster electrochemistry, for example in the clusters $[M_3(CO)_{12}]$ (M = Ru, Os).[39, 40] The redox behavior of **1** is quite different from that of $[Os_3(CO)_{10}(bpy)]$. The latter cluster undergoes metal-metal bond cleavage on reduction instead of a CO-loss reaction.[4, 38] However, in **1** one Os–Os bond is already broken, and the tmbp ligand, spanning the triosmium core, will prevent cleavage of a second metal–metal bond. Also, in **1** the triosmium core has become electron-deficient because of the oxidative "addition" of tmbp to the $\{Os_3(CO)_{10}\}$ moiety, which facilitates the substitution of a strong π-acceptor carbonyl group by the more basic PPh_3. In contrast to this, CO substitution by PPh_3 in $[Os_3(CO)_{10}(bpy)]$ cannot be achieved by thermal substitution or by radical-anion-mediated substitution (catalyzed by sodium biphenyl ketyl). The poorly electron-withdrawing 2,2′-bipyridine ligand makes the triosmium core too electron-rich for this reaction.[40] Instead, a thermal reaction of $[Os_3(CO)_{10}(L)]$ (L = bpy, dmb) with PPh_3 results in the substitution of the α-diimine, to produce $[Os_3(CO)_{10}(PPh_3)_2]$.[41]

Conclusion

The 50e$^-$ cluster $[Os_3(CO)_{10}(\mu_2\text{-}P,\mu_2\text{-}P'\text{-}tmbp)]$, **1**, and its PPh_3 derivative **2** show an unprecedented coordination mode of tmbp, with both P atoms bridging two metal atoms. The tmbp ligand is formally two-electron reduced by electron transfer from the cluster core, which is consistent with cleavage of one Os–Os bond. The electron-deficiency of the cluster core accounts for the facile electrocatalytic substitution of CO by more basic PPh_3 and other tertiary phosphanes and phosphites. The overall two-electron reduction of **1** and **2** leads to dissociation of CO and PPh_3, respectively, and to formation of the $[Os_3(CO)_9(tmbp)]^{2-}$ ion. The initially produced radical anions are fairly stable owing to localization of the odd electron on tmbp, which also clamps the triosmium core. DFT calculations on model clusters show that both the HOMO and LUMO of clusters **1** and **2** are largely localized on tmbp. The predominant intraligand character of the lowest excited state accounts for the observed photostability of the clusters. Time-dependent DFT calculations then facilitate interpretation of poorly resolved electronic absorption spectra of low-symmetry **1** and **2** in the visible region, which otherwise would remain a matter of considerable speculation. In general, this paper demonstrates the power of the recommendable combined experimental and theoretical approach in intriguing cluster chemistry that opens new perspectives in this field.

Experimental Section

Materials and preparations: $[Os_3(CO)_{12}]$ (ABCR) and PPh_3 (Aldrich) were used as purchased. Trimethylamine-*N*-oxide dihydrate, $Me_3NO \cdot 2H_2O$ (Alfa), was dehydrated before use by vacuum sublimation. Analytical grade solvents (Acros: hexane, dichloromethane, THF, toluene, acetonitrile, dimethoxyethane (DME)) and spectroscopic grade solvents (Aldrich: pyridine; Fluka: butyronitrile; Merck: CCl_4) were dried over sodium wire (hexane, THF, toluene, DME) or CaH_2 (dichloromethane, CCl_4, pyridine, acetonitrile, butyronitrile) and freshly distilled prior to use. Silica gel (Kieselgel 60, Merck, 70–230 Mesh), used for column chromatography, was activated by heating overnight under vacuum at 160 °C. Elemental analyses were carried out in the "Mikroanalytisches Laboratorium" of Dr. H. Kolbe (Müllheim an der Ruhr, Germany).

The ligand 4,4′,5,5′-tetramethyl-2,2′-biphosphinine (tmbp)[5], the 19-electron reducing agent $[Fe^{I}(\eta^5\text{-}C_5H_5)(\eta^6\text{-}C_6Me_6)]$, and its poorly soluble precursor $[Fe^{II}(\eta^5\text{-}C_5H_5)(\eta^6\text{-}C_6Me_6)]PF_6$[42] were prepared according to published procedures. The synthesis of the cluster $[Os_3(CO)_{10}(tmbp)]$ **1**, was communicated previously.[13]

Synthesis of $[Os_3(CO)_9(tmbp)(PPh_3)]$ (2): A solution of $[Os_3(CO)_{10}(tmbp)]$ (**1**) (87 mg, 0.079 mmol) and excess PPh_3 (62 mg, 0.24 mmol) in THF (60 mL) was stirred for 30 min. No thermal reaction was observed during this time. A catalytic amount of sodium diphenyl ketyl (5 %), prepared by addition of finely cut sodium metal to a solution of benzophenone (76 mg) in THF (5 mL), was then added. The solution was stirred for 5 min, and the solvent was evaporated under vacuum. The crude product was purified by column chromatography over silica. First, small amounts of unreacted **1** and excess PPh_3 were eluted with hexane/toluene 5:1, followed by the product in hexane/toluene 4:3. Pure **2** was obtained as a purple powder in 85 % yield. ^{1}H NMR ($CDCl_3$): $\delta = 7.39$ (m, 15 H; PPh_3), 6.85 (d, ^3J(P(1),H) = 19.2 Hz, 1 H; C(4)–H), 6.65 (d, ^3J(P(2),H) = 16.5 Hz, 1 H; C(9)–H), 6.39 (d, ^2J(P(2),H) = 31.8 Hz, 1 H; C(1)–H), 6.23 (d, ^2J(P(1),H) = 28.2 Hz, 1 H; C(6)–H), 2.13 (s, 6 H; 2 CH_3), 1.93 (s, 3 H; CH_3), 1.78 (s, 3 H; CH_3); ^{31}P{^{1}H} NMR ($CDCl_3$) δ: 25.5 (d, 1 P; P(2)), −7.64 (d, 1 P; P(3) of PPh_3), −134.4 (dd, ^2J(P(1),P(2)) = 109 Hz, ^2J(P(1),P(3)) = 310 Hz, 1 P; P(1)); IR (THF): $\tilde{\nu}$(CO) = 2061 (m), 2035 (s), 2002 (vs), 1987 (s), 1970 (m), 1958 (w), 1935(sh), 1930 (w) cm^{-1}; UV/Vis (THF): λ_{max} = 347 (sh), 455 (sh), 548, 593 (sh) nm; FAB MS: *m*/*z* (%): 1332.0 $[M]^+$; elemental analysis calcd (%) for $C_{41}H_{31}O_9Os_3P_3$ (1332.0): C 36.99, H 2.35, P 6.98; found: C 37.09, H 2.36, P 7.01.

Crystallography: Crystal data and details of the structure determination of cluster **2** are presented in Table 9. Crystals of $\mathbf{2} \cdot C_6H_{12}$ were grown by heating a solution of the complex in cyclohexane for five days at 80 °C. Data were collected at 150 K on a Nonius Kappa CCD diffractometer, using a $\lambda(Mo_{K\alpha}) = 0.71069$ Å X-ray source and a graphite monochromator. Multiple scan absorption corrections were applied. The crystal structure was solved using SIR 97[43] and refined with SHELXL-97.[44] The sample gave acceptable diffraction up to a relatively low Θ limit of 27°. Cluster **2** contains three osmium atoms; truncation errors in the Fourier synthesis gave rise to large positive and negative peaks near these atoms. In addition, the crystallographic data (Table SI 4 in Supporting Information) exhibit very strong anisotropic behavior of several atoms, for example C7, C8, C13, C14, C29, C30, O4, C42–C47. For C42–C47 this is understandable, as the cyclohexane solvate is highly agitated and its long-range order is poor; our model could not account for this fact. The other atoms in question are more puzzling and no definite explanation is given. Slight long-range disorder or systematic errors may be responsible for the observed elongation of some thermal parameters.

CCDC-168994 (**2**) contains the supplementary crystallographic data for this paper. These data can be obtained free of charge via www.ccdc.cam.ac.uk/conts/retrieving.html (or from the Cambridge Crystallographic Data Centre, 12 Union Road, Cambridge CB2 1EZ, UK (fax: (+44) 1223-336-033; e-mail: deposit@ccdc.cam.ac.uk).

Computational details: All Density Functional Theory calculations[14] were performed by using the Amsterdam Density Functional program package (ADF-2.3 and ADF99).[15, 45] The local spin density (LSD) exchange correlation potential was used with the local density approximation of the correlation energy (Vosko–Wilk–Nusair).[46] Furthermore, Becke's nonlocal corrections[47, 48] to the exchange energy and Perdew's nonlocal corrections[49, 50] to the correlation energy were included in the calculation of the gradients. Relativistic effects were treated by a quasirelativistic method in which Darwin and mass-velocity terms are incorporated[51–53] in the energy optimizations, and using the ZORA[28] formalism in the TD DFT calculations.[27] The inner shells of the Os (1s-5p), P (1s-2p), C (1s), and O (1s) atoms were frozen. A triple-ζ STO basis set was used for the valence part of the Os atoms (5d, 6s, 6p). The 2s and 2p valence shells of the C atoms, as well as the 3s, 3p valence shells of the P atoms, were described by a triple-ζ STO basis, augmented by one 3d polarization function. For the O (2s, 2p) and H (1s) atoms a double-ζ STO basis was used. When using ADF99 and ZORA, a frozen Os (1s-4f) core was used, as well as the ZORA wavefunctions within the ADF program for all atoms.

The geometry optimizations were performed without any symmetry constraints. The X-ray structures of complexes **1** and **2** were used to build models, **1A** and **1B**, respectively, in which the methyl groups were replaced by hydrogen atoms. The X-ray structure of $[Os_3(CO)_{10}(bpy)]$[54] was used to model the other studied isomers of **1A**.

Spectroscopic measurements: FTIR spectra were recorded on Bio-Rad FTS-7 spectrometer, UV/Vis absorption spectra on a Hewlett Packard 8453 diode-array spectrophotometer, NMR spectra on a Bruker AMX 300 spectrometer (300.13 MHz), and FAB mass spectra on a JEOL JMS SX/SX102A four-sector mass spectrometer coupled to a JEOL MS-MP 7000 data system.

Spectroelectrochemistry: Cyclic voltammetry was performed in a single compartment vacuum-tight cell under an atmosphere of dry argon. The cell was equipped with Pt disc working (apparent surface area of 0.42 mm^2), Pt wire auxiliary, and Ag wire pseudoreference electrodes. The working electrode was carefully polished with a 0.25 μm grain diamond paste. All redox potentials are reported against the ferrocene-ferrocenium (Fc/Fc^+) redox couple used as an internal standard.[55] The solutions for cyclic voltammetric experiments were typically 5×10^{-4} M in the cluster compounds and 10^{-1} M in Bu_4NPF_6. The potential control was achieved with a PAR Model 283 potentiostat. Infrared spectroelectrochemical experiments at variable temperature were performed with optically transparent thin-layer electrochemical (OTTLE) cells,[56, 57] equipped with a Pt minigrid working electrode (32 wires/cm) and CaF_2 optical windows. The spectro-

Table 9. Crystallographic data and experimental parameters for cluster **2**.

molecular formula	$C_{41}H_{30}Os_3P_3.C_6H_{12}$
molecular weight	1414.32
crystal habit	red plate
crystal dimensions [mm]	0.16 × 0.07 × 0.04
crystal system	triclinic
space group	$P\bar{1}$
a [Å]	11.599(5)
b [Å]	11.936(5)
c [Å]	17.561(5)
α [°]	78.220(5)
β [°]	84.330(5)
γ [°]	76.830(5)
V [Å^3]	2314.0(15)
Z	2
ρ_{calcd} [g cm^{-3}]	2.030
F(000)	1338
μ [cm^{-1}]	8.374
max Θ [°]	27.44
hkl ranges	−15 13 ; −15 15 ; −22 22
reflections measured	15390
indepedent reflections	10491
reflections used	8291
R_{int}	0.0452
refinement type	Fsqd
hydrogen atoms	constrained
parameters refined	563
reflections/parameter	14
*wR*2	0.0818
*R*1	0.0411
GoF	0.995
weights a,b1	0.0253; 0.0000
difference peak/hole [eÅ^{-3}]	2.260(0.219)/2.452(0.219)

0947-6539/02/0807-1750 $ 20.00+.50/0 *Chem. Eur. J.* **2002**, *8*, No. 7

electrochemical samples were typically 5×10^{-3} M in the cluster compounds. A PA4 potentiostat (EKOM, Czech Republic) was used to carry out the controlled-potential electrolyses.

Acknowledgements

Mr. M. de Groot is thanked for his assistance with the electrocatalytic study of cluster **1**. M.J.C. and F.H. gratefully acknowledge funding from the TMR Network 'Metal Clusters in Catalysis and Organic Synthesis'. This work has also been undertaken as a part of the European collaborative COST project (D14/0001/99). Financial support has also been received from the Council for Chemical Sciences of the Netherlands Organization for Scientific Research (CW-NWO, project No. 348–032; F.W.V. and F.H.) and from the CNRS and the École Polytechnique (P.R., L.R. and P.L.F.). M.J.C. thanks Dr. S.J.A. van Gisbergen (Vrije Universiteit, Amsterdam) for helpful discussions regarding the ADF programs.

[1] J. W. M. van Outersterp, M. T. Garriga Oostenbrink, H. A. Nieuwenhuis, D. J. Stufkens, F. Hartl, *Inorg. Chem.* **1995**, *34*, 6312.
[2] J. Nijhoff, M. J. Bakker, F. Hartl, D. J. Stufkens, W.-F. Fu, R. van Eldik, *Inorg. Chem.* **1998**, *37*, 661.
[3] J. W. M. van Outersterp, PhD thesis, University of Amsterdam, **1995**.
[4] J. Nijhoff, F. Hartl, J. W. M. van Outersterp, D. J. Stufkens, M. J. Calhorda, L. F. Veiros, *J. Organomet. Chem.* **1999**, *573*, 121.
[5] P. Le Floch, D. Carmichael, L. Ricard, F. Mathey, *J. Am. Chem. Soc.* **1991**, *113*, 667.
[6] F. Mathey, P. Le Floch, *Chem. Ber.* **1996**, *129*, 263.
[7] a) P. Le Floch, F. Mathey, *Coord. Chem. Rev.* **1998**, *179–180*, 771; b) N. Mézailles, F. Mathey, P. Le Floch, *Progr. Inorg. Chem.* **2001**, *49*, 455.
[8] P. Le Floch, D. Carmichael, L. Ricard, F. Mathey, A. Juttand, C. Amatore, *Organometallics* **1992**, *11*, 2475.
[9] a) P. Le Floch, L. Ricard, F. Mathey, A. Juttand, C. Amatore, *Inorg. Chem.* **1995**, *34*, 11; b) S. Choua, H. Sidorenkova, T. Berclaz, M. Geoffroy, P. Rosa, N. Mézailles, L. Ricard, F. Mathey, P. Le Floch, *J. Am. Chem. Soc.* **2000**, *122*, 12227.
[10] P. Rosa, N. Mézailles, L. Ricard, F. Mathey, P. Le Floch, *Angew. Chem.* **2000**, *112*, 1893; *Angew. Chem. Int. Ed.* **2000**, *39*, 1823.
[11] P. Rosa, L. Ricard, P. Le Floch, F. Mathey, G. Sini, O. Eisenstein, *Inorg. Chem.* **1998**, *37*, 3154.
[12] P. Rosa, N. Mézailles, L. Ricard, F. Mathey, P. Le Floch, Y. Jean, *Angew. Chem.* **2001**, *113*, 1291; *Angew. Chem. Int. Ed.* **2001**, *40,* 1251.
[13] M. J. Bakker, F. W. Vergeer, F. Hartl, K. Goubitz, J. Fraanje, P. Rosa, P. Le Floch, *Eur. J. Inorg. Chem.* **2000**, 843.
[14] R. G. Parr, W. Yang, *Density Functional Theory of Atoms and Molecules*, Oxford University Press, New York, **1989**.
[15] E. J. Baerends, A. Bérces, C. Bo, P. M. Boerrigter, L. Cavallo, L. Deng, R. M. Dickson, D. E. Ellis, L. Fan, T. H. Fischer, C. Fonseca Guerra, S. J. A. van Gisbergen, J. A. Groeneveld, O. V. Gritsenko, F. E. Harris, P. van den Hoek, H. Jacobsen, G. van Kessel, F. Kootstra, E. van Lenthe, V. P. Osinga, P. H. T. Philipsen, D. Post, C. C. Pye, W. Ravenek, P. Ros, P. R. T. Schipper, G. Schreckenbach, J. G. Snijders, M. Sola, D. Swerhone, G. te Velde, P. Vernooijs, L. Versluis, O. Visser, E. van Wezenbeek, G. Wiesenekker, S. K. Wolff, T. K. Woo, T. Ziegler, *ADF99,* Vrije Universiteit, Amsterdam, **1999**.
[16] P. Rosa, PhD thesis, École Polytechnique, Palaiseau (France), **2000**.
[17] Average values for inter-ring C–C and P–C distances (Å in $[W(tmbp)_3]$ (ref. [9b]): C–C, 1.445(4), P–C, 1.725(3) external, 1.737(6) internal; $[Zr(tmbp)_3]^{2-}$ (ref. [10]): C–C, 1.435(4), P–C, 1.752(3) external, 1.780(3) internal; $[Mn(CO)_3(tmbp)]^-$ (ref. [18]): C–C, 1.434(4), P–C, 1.728(3) external, 1.754(3) internal.
[18] F. Hartl, T. Mahabiersing, P. Le Floch, F. Mathey, P. Rosa, L. Ricard, S. Záliš, unpublished results.
[19] B. Schmid, L. Venanzi, T. Gerfin, V. Gramlich, F. Mathey, *Inorg. Chem.* **1992**, *31*, 5117.
[20] A. J. Arce, A. J. Deeming, Y. De Sanctis, J. Manzur, *J. Chem. Soc. Chem. Commun.* **1993**, 325.
[21] P. Rosa, L. Ricard, F. Mathey, P. Le Floch, *Organometallics* **2000**, *19*, 5247.
[22] A. J. Arce, P. Arrojo, Y. De Sanctis, A. J. Deeming, D. J. West, *Polyhedron* **1992**, *11*, 1013.
[23] J. Zhang, W. K. Leong, *Dalton Trans.* **2000**, 1249.
[24] A. J. Deeming in *Comprehensive Organometallic Chemistry II, Vol. 7* (Eds.: D. F. Shriver, M. I. Bruce), Pergamon, Oxford, **1995**, p. 690.
[25] E. Hunstock, C. Mealli, M. J. Calhorda, J. Reinhold, *Inorg. Chem.* **1999**, *38*, 5053.
[26] M. J. Calhorda, E. Hunstock, L. F. Veiros, F. Hartl, *Eur. J. Inorg. Chem.* **2001**, 223.
[27] a) T. Ziegler, A. Rauk, *Inorg. Chem.* **1979**, *18*, 1755; b) T. Ziegler, A. Rauk, *Inorg. Chem.* **1979**, *18*, 1758; c) T. Ziegler, A. Rauk, *Theor. Chim. Acta* **1977**, *46*, 1.
[28] C. Elschenbroich, A. Salzer, *Organometallics: A Concise Introduction*, VCH, Weinheim, **1989**.
[29] a) S. J. A. van Gisbergen, J. A. Groeneveld, A. Rosa, J. G. Snijders, E. J. Baerends, *J. Phys. Chem. A* **1999**, *103*, 6835; b) A. Rosa, E. J. Baerends, S. J. A. van Gisbergen, E. van Lenthe, J. A. Groeneveld, J. G. Snijders, *J. Am. Chem. Soc.* **1999**, *121*, 10356; c) S. J. A. van Gisbergen, A. Rosa, G. Ricciardi, E. J. Baerends, *J. Chem. Phys.* **1999**, *111*, 2499.
[30] E. van Lenthe, A. Ehlers, E. J. Baerends, *J. Chem. Phys.* **1999**, *110*, 8943.
[31] M. J. Bakker, F. Hartl, E. Hunstock, M. J. Calhorda, unpublished results.
[32] Determination of the apparent number of electrons n_{app} involved in the reduction of **1** at room temperature, with the method described by Amatore and co-workers (see C. Amatore, M. Azzabi, P. Calas, A. Jutand, C. Lefrou, Y. J. Rollin, *Electroanal. Chem.* **1990**, *288*, 45) gave too high a value of $n_{app} = 2.5$. However, comparison of the anodic peak current of the $1e^-$ oxidation wave of the internal standard ferrocene with those of the reduction wave of **1** both at 223 K ($1e^-$ process) and at room temperature, confirm that reduction of **1** at the room temperature involves transfer of two electrons. This is also in agreement with the formation of product **B′** from the reactive dianion $\mathbf{1}^{2-}$ at low temperatures.
[33] J. A. Krause, U. Siriwardane, T. A. Salupo, J. R. Wermer, D. W. Knoeppel, S. G. Shore, *J. Organomet. Chem.* **1993**, *454*, 263.
[34] D. Osella, C. Nervi, M. Ravera, J. Fiedler, V. V. Strelets, *Organometallics* **1995**, *14*, 2501.
[35] D. Astruc, *Electron Transfer and Radical Processes in Transition Metal Chemistry,* VCH, New York, **1995**.
[36] J. W. Hershberger, R. J. Klingler, J. K. Kochi, *J. Am. Chem. Soc.* **1983**, *105*, 61.
[37] The substitution products $[Os_3(CO)_9(tmbp)(PR_3)]$ are all reduced at similar electrode potentials: $E_{p,c} = -1.93$ V (R = Ph); -1.91 V (R = Et); -1.93 V (R = cyclohexyl); -1.89 V (R = OPh) vs. Fc/Fc^+ (cyclic voltammetry, $v = 100$ mVs^{-1} room temperature). This result points to the limited influence of the phosphorus ligands on the character of the LUMO of $[Os_3(CO)_9(tmbp)(PR_3)]$ (less than 5% contribution), in agreement with the preceding DFT calculations on model **2A**.
[38] F. Hartl, J. W. M. van Outersterp, unpublished results.
[39] A. J. Downard, B. H. Robinson, J. Simpson, A. M. Bond, *J. Organomet. Chem.* **1987**, *320*, 363.
[40] J. E. Cyr, P. H. Rieger, *Organometallics* **1991**, *10*, 2153.
[41] M. J. Bakker, F. W. Vergeer, F. Hartl, unpublished results. Typically, the reaction mixture of $[Os_3(CO)_{10}(dmb)]$ and two equivalents of PR_3 (R = Ph, cyclohexyl) in dichloromethane contains only uncoordinated 4,4′-dimethyl-2,2′-bipyridine after stirring at room temperature for five hours: ^{1}H NMR (CD_2Cl_2): $\delta = 8.54$ (d), 8.23 (d), 7.15 (d), 2.44 (s). The IR ν(CO) spectrum of the major carbonyl product agreed with that of $[Os_3(CO)_{10}(PPh_3)_2]$: W. K. Leong, Y. Liu, *J. Organomet. Chem.* **1999**, *584*, 174.
[42] D. Astruc, M. Hamon, M. Lacoste, M.-H. Desbois, E. Roman, E. in *Organometallic Synthesis, Vol. IV* (Ed.: R. B. King), Elsevier, Amsterdam, **1988**, p. 172.
[43] SIR97, an integrated package of computer programs for the solution and refinement of crystal structures using single-crystal data: A. Altomare, M. C. Burla, M. Camalli, G. Gascarno, C. Giacovazzo, A. Guagliardi, A. G. G. Moliterni, G. Polidori, R. Spagna.
[44] G. M. Sheldrick, SHELXL-97, Programs for Crystal Structure Analysis (Release 97–2); Universität Göttingen: Göttingen, Germany, **1998**.

[45] a) C. Fonseca Guerra, O. Visser, J. G. Snijders, G. te Velde, E. J. Baerends, *Parallelization of the Amsterdam Density Functional Programme* in: *Methods and Techniques for Computational Chemistry* (Eds.: E. Clementi, C. Corongiu), STEF, Cagliari, **1995**, pp. 303 – 395; b) C. Fonseca Guerra, J. G. Snijders, G. te Velde, E. J. Baerends, *Theor. Chem. Acc*. **1998**, *99,* 391; c) E. J. Baerends, D. Ellis, P. Ros, *Chem. Phys.* **1973**, *2*, 41; d) E. J. Baerends, P. Ros, *Int. J. Quantum Chem*. **1978**, *S12*, 169; e) P. M. Boerrigter, G. te Velde, E. J. Baerends, *Int. J. Quantum Chem*. **1988**, *33*, 87; f) G. te Velde, E. J. Baerends, *J. Comp. Phys.* **1992**, *99*, 84.
[46] S. H. Vosko, L. Wilk, M. J. Nusair, *Can. J. Phys.* **1980**, *58*, 1200.
[47] A. D. Becke, *J. Chem. Phys.* **1986**, *84*, 4524.
[48] A. D. Becke, *Phys. Rev. B* **1988**, *38*, 3098.
[49] P. J. Perdew, *Phys. Rev. B* **1986**, *33*, 8822.
[50] P. J. Perdew, *Phys. Rev. B* **1986**, *34*, 7406.
[51] T. Ziegler, V. Tschinke, E. J. Baerends, J. G. Snijders, W. Ravenek, *J. Phys. Chem.* **1989**, *93*, 3050.
[52] J. G. Snijders, E. J. Baerends, *Mol. Phys.* **1978**, *36*, 1789.
[53] J. G. Snijders, E. J. Baerends, P. Ros, *Mol. Phys.* **1979**, *38*, 1909.
[54] N. E. Leadbeater, J. Lewis, P. R. Raithby, G. N. Ward, *J. Chem. Soc. Dalton Trans.* **1997**, 2511.
[55] G. Gritzner, J. Kůta, *Pure Appl. Chem.* **1984**, *56*, 461.
[56] M. Krejčk, M.Daněk, F. Hartl, *J. Electroanal. Chem., Interfacial Electrochem.* **1991**, *317*, 179.
[57] F. Hartl, H. Luyten, H. A. Nieuwenhuis, G. C. Schoemaker, *Appl. Spectrosc*. **1994**, *48*, 1522.

Received: September 7, 2001 [F3539]

  0947-6539/02/0807-1752 $ 20.00+.50/0